Supplementary Information (SI) for Lab on a Chip.
This journal is © The Royal Society of Chemistry 2025

Supplementary Information for

Gravity-induced tunable asymmetric droplet splitting for flexible and precise reagent formulation on vertical digital microfluidics.

Note I. Analysis of droplet detection algorithm

In gravity-coupled digital microfluidic experiments, droplet faces challenges such as unstable illumination, complex backgrounds, and variations in droplet morphology. Conventional image-processing methods rely on hand-crafted features and struggle to maintain stability and real-time performance under these conditions. YOLO models, with their end-to-end deep learning architecture, enable fast and accurate object detection and can effectively handle multi-scale targets with low contrast or blurred boundaries. Their strong robustness and generalization capability make them well suited for tasks such as droplet localization and state monitoring, thereby reducing errors caused by experimental fluctuations and providing reliable inputs for downstream control and analysis.

As the most recent version in the YOLO family, YOLOv11 incorporates structural and feature-processing enhancements to further improve detection performance. The C3K2 module strengthens feature representation while maintaining a lightweight design. The SPFF structure enhances multi-scale information fusion through rapid spatial pyramid pooling, making the model more capable of detecting droplets with varying sizes and shapes. The C2PSA attention mechanism increases the response to critical regions, resulting in higher detection accuracy. With improved real-time performance, reduced computational cost, and more stable outputs, YOLOv11 remains reliable even under complex backgrounds or interference, and is therefore adopted as the core detection algorithm in this study.

Note II. Derivation of the relationship between droplet size threshold and gap height

In vertical DMF chips, friction on droplets is caused by contact angle hysteresis. The maximum friction force (F_c) can be determined from the advancing contact angle (θ_A) and receding contact angle (θ_R):

$$F_C = 2\gamma D(\cos\theta_R - \cos\theta_A) \tag{1}$$

Here γ is the surface tension between liquid and air, D represents the diameter of droplets. The droplet gravity can be calculated as follows:

$$G = \frac{\pi}{4} D^2 \cdot d \cdot \rho g \tag{2}$$

Here d is the gap height of DMF chip, ρ is the droplet density, and g is gravitational acceleration. For a droplet stably resting on the chip surface, F_c is greater than or equal to G, that is:

$$2\gamma D(\cos\theta_R - \cos\theta_A) \geq \frac{\pi}{4} D^2 \cdot d \cdot \rho g \tag{3}$$

Thus the relationship between the diameter w and gap height d can be derived as follows:

$$D \cdot d \leq \frac{8\gamma}{\pi \cdot \rho g}(\cos\theta_R - \cos\theta_A) \tag{4}$$

Since θ_A and θ_R are determined solely by the properties of the solid–liquid interface, and γ, ρ, and g are constant. As a result, d is inversely related to D.

Note III. Theoretical analysis of conventional droplet splitting on DMF chip

According to the Laplace equation, the droplet pressure P at each part can be described as:

$$P_1 - P_0 = \gamma\left(\frac{1}{r_1} + \frac{1}{R_1}\right) \tag{5}$$

$$P_2 - P_0 = \gamma\left(\frac{1}{r_2} + \frac{1}{R_2}\right) \tag{6}$$

$$P_3 - P_0 = \gamma\left(\frac{1}{r_3} + \frac{1}{R_3}\right) \tag{7}$$

Where P_0 is the atmosphere pressure, P_2 is the pressure of the liquid bridge, P_1 and P_3 are the pressures at both ends of the dumbbell-shaped droplet, respectively. R is the principal radius of curvature as shown in Fig. 3(b) (i). For the geometric relationship as shown in Fig. 3(a), the pressure differential between each part can be expressed as:

$$P_2 - P_1 = \gamma\left(\frac{1}{R_2} - \frac{1}{R_1} + \frac{\cos\theta_v - \cos\theta_0}{d}\right) \tag{8}$$

$$P_2 - P_3 = \gamma\left(\frac{1}{R_2} - \frac{1}{R_3} + \frac{\cos\theta_v - \cos\theta_0}{d}\right) \tag{9}$$

Here, θ_0 and θ_v denote the contact angle on the bottom plate without and with applied voltage, respectively; d is the gap height between two plates. As the droplet is on the same horizontal plate, the pressure should be equal inside the droplet in a state of static equilibrium. There is:

$$P_2 - P_1 = P_2 - P_3 = 0 \tag{10}$$

Substituting Equation (8) and (9) into Equation (10), it can be derived during the splitting process:

$$R_1 = R_3 \tag{11}$$

Therefore, conventional droplet splitting method enable the production of two daughter droplets with uniform size.

Note IV. Analysis of the agreement between theoretical and experimental results for gravity-induced asymmetric splitting

In this study, DI water with a surface tension of 72 mN/m was used. When the curvature radius R at the two ends of the dumbbell-shaped droplet equals the half of the splitting electrode side length (i.e. 500 μm), and the height differences H_1 and H_2 are approximately 1500 μm, the right-hand side of Equation (19) and (20) in Section 3.2 become:

$$\frac{1}{R_1} + \frac{\rho g H_1}{\gamma} = 2204.17(m^{-1}) \tag{12}$$

$$\frac{1}{R_3} - \frac{\rho g H_2}{\gamma} = 1795.83(m^{-1}) \tag{13}$$

Where the density of water ρ is 10^3 Kg/m^3, the gravitational acceleration g is 9.8 m/s^2. As shown in Fig. S2(a), the contact angle of droplet on CYTOP coated surface is 110°, the advancing and receding contact angles are 114° and 106°, respectively, indicating that the contact angle variation α introduced by random pinning forces is 4°.[1] Therefore, the applied-voltage contact angle θ_v required to satisfy the generation conditions of the UD and LD are, respectively:

$$\theta_{\mathrm{v\_UD}} < 89.17° \tag{14}$$

$$\theta_{\mathrm{v\_LD}} < 91.45° \tag{15}$$

This successfully confirms that, under practical conditions, the generation of the LD is easier than that of the UD. The voltage-independent contact angle variation is shown in Fig. S2(b). The voltages corresponding to θ_v = 89.17°, 91.45° fall within the range of 140 - 150 Vpp, demonstrating excellent agreement with the actual actuating voltages applied in the experiments.

Note V. Conversion steps between contact line lengths and pixel coordinates

The outcome of droplet splitting is directly related to the contact line length between the droplet and the splitting electrode. Consequently, conversion of the droplet coordinates obtained through image recognition algorithms is required. As illustrated in Fig. S5, the cross-section of the naturally sliding droplet is approximated as a circle throughout the entire process. Here, x_0, y_0 denote the coordinate position of the splitting electrode center; x_1, x_2 represent the horizontal coordinates of the droplet's leftmost and rightmost points; y_1, y_2 indicate the vertical coordinates of the droplet's topmost and bottommost points; r signifies the droplet radius; w represents the electrode side length; h denotes the distance between two adjacent electrodes; and l defines the contact line length between the droplet and the electrode. According to the Pythagorean theorem:

$$r^2 = \left(\frac{l}{2}\right)^2 + \left(h + \frac{w}{2} + \left|y_0 - \frac{y_1 + y_2}{2}\right|\right)^2 \tag{16}$$

Where the radius r can be expressed as a function of y_1 and y_2:

$$r = \frac{y_1 - y_2}{2} \tag{17}$$

Substituting Equation (16) into Equation (17) gives:

$$\left(\frac{l}{2}\right)^2 = \left(\frac{y_1 - y_2}{2}\right)^2 - \left(h + \frac{w}{2} + \left|y_0 - \frac{y_1 + y_2}{2}\right|\right)^2 \tag{18}$$

When the droplet is positioned lower (Fig. S5(a)), the contact line length l_1 between the droplet and the upper splitting electrode can be expressed as:

$$\left(\frac{l}{2}\right)^2 = \left(\frac{y_1 - y_2}{2}\right)^2 - \left(h + \frac{w}{2} + y_0 - \frac{y_1 + y_2}{2}\right)^2 \tag{19}$$

When the droplet is positioned higher (Fig. S5(b)), the contact line length l_2 between the droplet and the lower splitting electrode can be expressed as:

$$\left(\frac{l}{2}\right)^2 = \left(\frac{y_1 - y_2}{2}\right)^2 - \left(h + \frac{w}{2} - y_0 + \frac{y_1 + y_2}{2}\right)^2 \tag{20}$$

Note VI. Normalized and matching steps for true and predicted y coordinates of droplets

For the ground-truth annotations, the coordinates of droplet centers (x_{center}, y_{center}) are already normalized to the range [0,1], where 0 and 1 correspond to the top and bottom edges of the image, respectively. Thus, the normalized ground-truth value can be written as:

$$y_{true,norm} = y_{center} \in [0,1] \tag{21}$$

For the predicted results, the bounding boxes are given in pixel coordinates (x_1, y_1, x_2, y_2). The vertical center of each bounding box is first computed as:

$$y_{pred,center} = \frac{y_1 + y_2}{2} \tag{22}$$

and then normalized:

$$y_{pred,norm} = \frac{y_{pred,center}}{H} = \frac{y_1 + y_2}{2H}, y_{pred,norm} \in [0,1] \tag{23}$$

Here, H is the image height. In this way, both the ground-truth and predicted y-coordinates are expressed on the same normalized scale [0,1], which enables direct comparison in error analysis and visualization.

In multiple droplet detection, the numbers of predicted boxes and ground-truth labels may be the same, but their orders sometimes differ; directly pairing them by index can therefore lead to mismatches. To address this issue, the Hungarian algorithm was employed to perform optical matching between predicted and ground-truth droplets for each image. The cost matrix C is constructed as Euclidean $C_{i,j}$, which is defined as :

$$C_{i,j} = \left\| t_i - p_j \right\|_2 = \sqrt{\left(x_i^{(t)} - x_j^{(p)}\right)^2 + \left(y_i^{(t)} - y_j^{(p)}\right)^2} \tag{24}$$

Where t_i and p_j is the center coordinate of the ground-truth and the predicted droplet, respectively. x and y means the x coordinate and y coordinate, respectively. To achieve a one-to-one optimal assignment, we define an assignment variable matrix:

$$X = [x_{i,j}] \tag{25}$$

Where

$$x_{i,j} = \begin{cases} 1, & t_i \quad assigned \quad to \quad p_j \\ 0, & otherwise \end{cases} \tag{26}$$

The linear assignment problem is then formulated as

$$\min_X \sum_i \sum_j C_{ij} x_{ij} \tag{27}$$

The constrains are:

$$\sum_j x_{ij} = 1, \quad \forall i; \quad \sum_i x_{ij} = 1, \quad \forall j. \tag{28}$$

By performing row reduction, column reduction, zero covering, and matrix adjustment, the original cost matrix is transformed into an equivalent simplified matrix, from which the assignment matrix X that satisfies all constraints and minimizes the total cost is ultimately obtained, thereby enabling an accurate correspondence between predicted and ground truth droplets.

Note VII. Analysis of the sensitivity of splitting accuracy to detection error

Experiments in Section 3.3 have demonstrated that the splitting results are not strongly related to the contact line ratios when the droplets are positioned lower at the start of the splitting process. Therefore, the influence of the detection deviation on the splitting results is mainly considered for cases where the droplet is positioned higher. According to the Equation (20) in Note V, the actual contact line length l_{act} and the detected contact line length l_{det} can be calculated as :

$$\left(\frac{l_{act}}{2}\right)^2 = \left(\frac{y_{1,act} - y_{2,act}}{2}\right)^2 - \left(h + \frac{w}{2} - y_0 + \frac{y_{1,act} + y_{2,act}}{2}\right)^2 \tag{29}$$

$$\left(\frac{l_{\mathrm{det}}}{2}\right)^2 = \left(\frac{y_{1,\mathrm{det}} - y_{2,\mathrm{det}}}{2}\right)^2 - \left(h + \frac{w}{2} - y_0 + \frac{y_{1,\mathrm{det}} + y_{2,\mathrm{det}}}{2}\right)^2 \tag{30}$$

Where the subscript “act” means the actual coordinate position, and the subscript “det” means the detected coordinate position. By combining Equations (29) and (30), the contact line deviation Δl is expressed as a function of the y-detection error, Δy_1 and Δy_2, whose definitions are as follows:

$$\Delta y_1 = y_{1,act} - y_{1,\mathrm{det}} \tag{31}$$

$$\Delta y_2 = y_{2,act} - y_{2,\mathrm{det}} \tag{32}$$

Since the droplet is initially positioned higher, the upper contact line length remains constant at 1000 µm. Therefore, the contact ratio error Δl_{rat} can be calculated from the error in the computed contact line length:

$$\Delta l_{rat} = \Delta l / 1000 \tag{33}$$

By substituting l_{rat} into the fitted curve in Fig. 4e, the deviation of the two sub-droplets ratio ΔV_{rat} is obtained:

$$\Delta V_{rat} = 0.805\Delta\left(l_{rat}^2\right) - 0.443\Delta l_{rat} \tag{34}$$

As shown in Fig. S7(c), most of the detection errors are within 8 pixels, and the corresponding error of contact line length is within 30 µm in reality. To further demonstrate the splitting sensitivity, we evaluated the splitting results under a higher microscope magnification when the upper-to-lower contact line ratios of 1000:650 and 1000:620 (Fig. S7(d)). The volume fractions of the two daughter droplets are 58.52% to 41.48% and 62.18% to 37.82%, respectively. The corresponding volume ratios are 1.41 and 1.64, which agree well with the fitted values of 1.48 and 1.63. Therefore, the maximum detection error in this work results in a splitting sensitivity error of approximately 3.66%. In future studies, this value can be further reduced by using higher microscope magnification or clearer imaging techniques.

Table S1 Summary of Splitting Characteristics for Different Strategies

Splitting Strategy	CV	Max. Ratio	Volume Range	Tunability	Electrode Design	Chip Modification
Open-Chip Droplet Splitting[2]	/	/	/	Tunable	No	No
Sub-electrode Arrays[3]	1% to 5%	/	7 from 150 nL	Fixed	Yes	No
Circular-arc electrodes[4]	<2%	42.7:57.3	/	Fixed	Yes	No
“One-to-three” Strategy[5]	1.64% to 3.71%	Electrode to Gap: 2.2	/	Fixed	Yes	No
Zigzag row-electrode[6]	1.26%	50:50	6 to 8 nL	Fixed	Yes	No
Virtual Microwells[7]	0.7% to 13.8%	/	80 to 800 nL	Fixed	No	Yes
Microblade Structure[8]	<2%	20:80	/	Fixed	Yes	Yes
Satellite Droplet Ejection[9]	/	/	picoliter to nanoliter	Tunable	Yes	Yes
Gravity Induced Splitting (GITS)	**<3%**	**12:88**	**17 to 120 nL**	**Tunable**	**No**	**No**

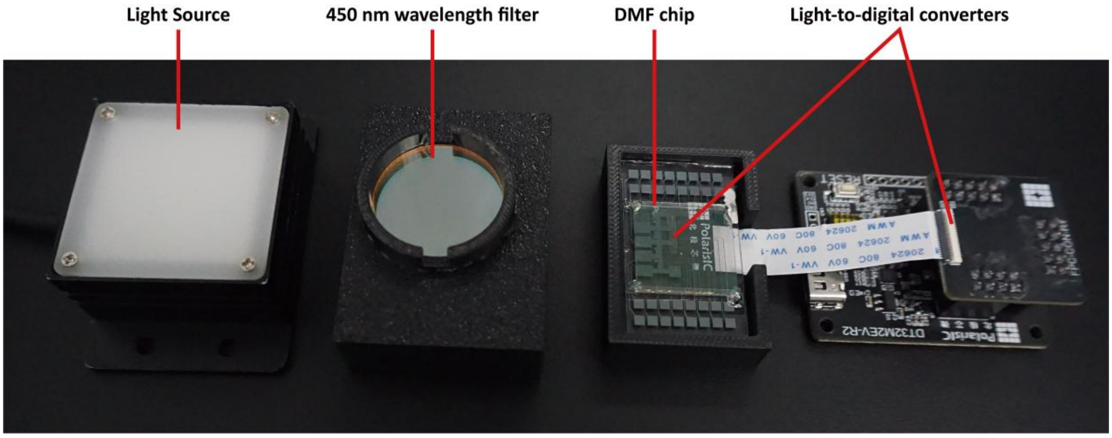

Fig. S1 On-chip cell quantification system. The system consisted of four parts: the light source, a 450 nm wavelength filter, a 3D printed supporter used to place chip and to provide a dark environment, and a light to digital converter.

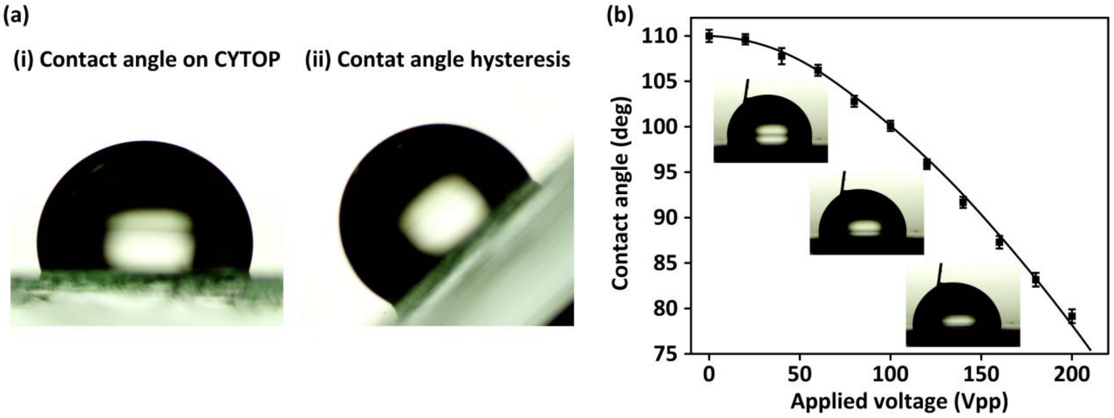

Fig. S2 Contact angles of droplets on CYTOP. (a)(i) Static contact angle of DI water on a CYTOP coated surface: 110°; (b) Contact angle hysteresis of DI water on CYTOP, showing an advancing angle of 114° and a receding angle of 106°. (b) Contact angles of a drop under AC actuation (1 kHz square signal).

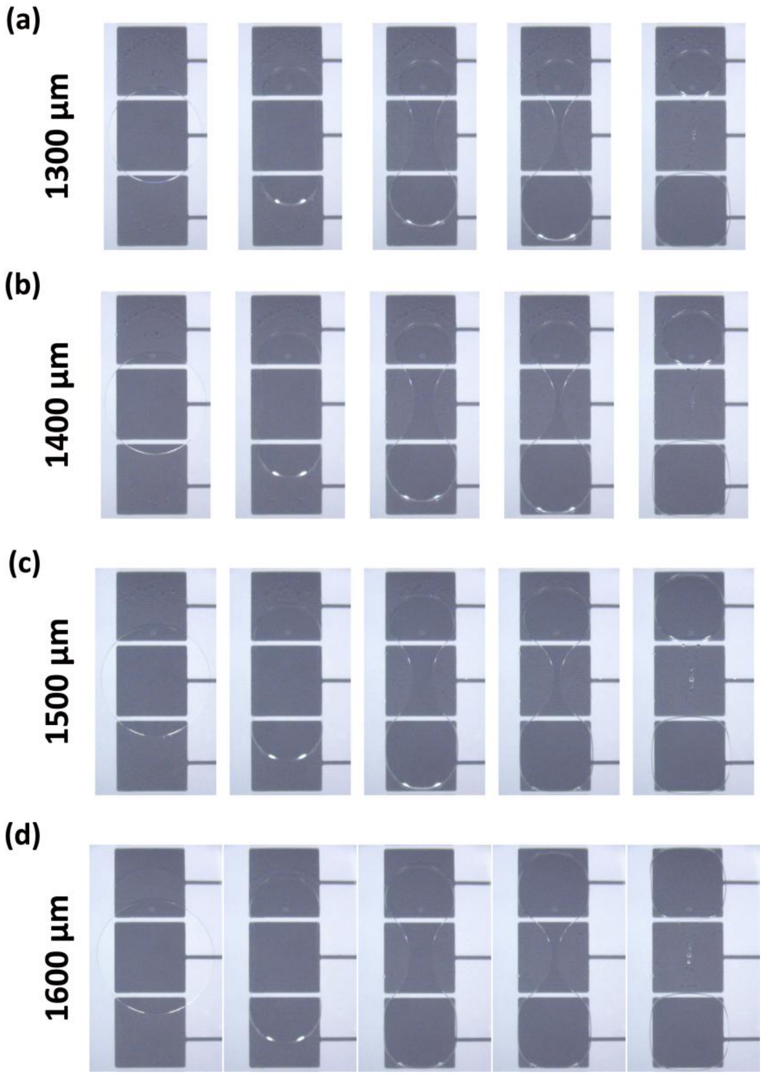

Fig. S3 Gravity-assisted splitting processes with diameters of (a) 1300 μm, (b) 1400 μm, (c) 1500 μm, and (d) 1600 μm, respectively. During the splitting process, fluid preferentially filled the bottom electrode. For larger droplet volumes, rupture of the connecting bridge was primarily caused by upward stretching of the upper liquid.

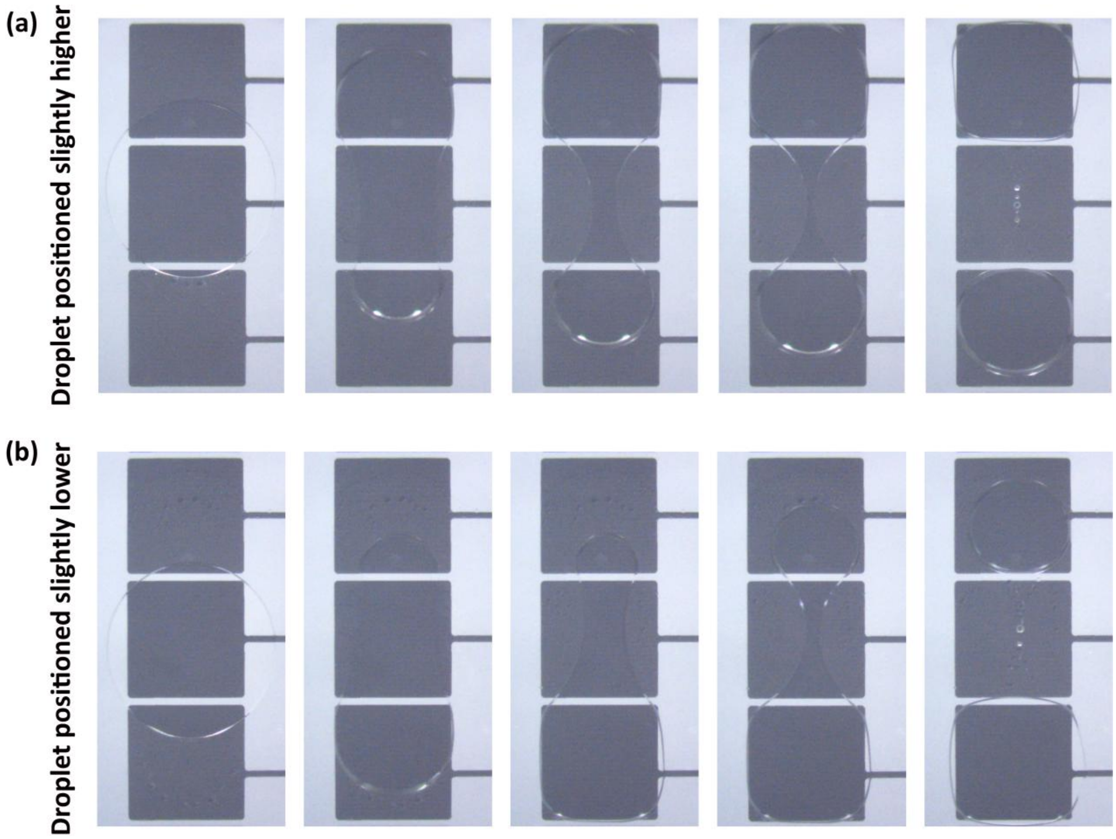

Fig. S4 Gravity-assisted splitting processes at a (a) higher position and a (b) lower position. When the droplet was positioned higher, splitting occurred during bidirectional stretching of the fluid. However, when the initial position was lower, the fluid preferentially filled the bottom electrode first, ultimately leading to upward stretching-induced rupture.

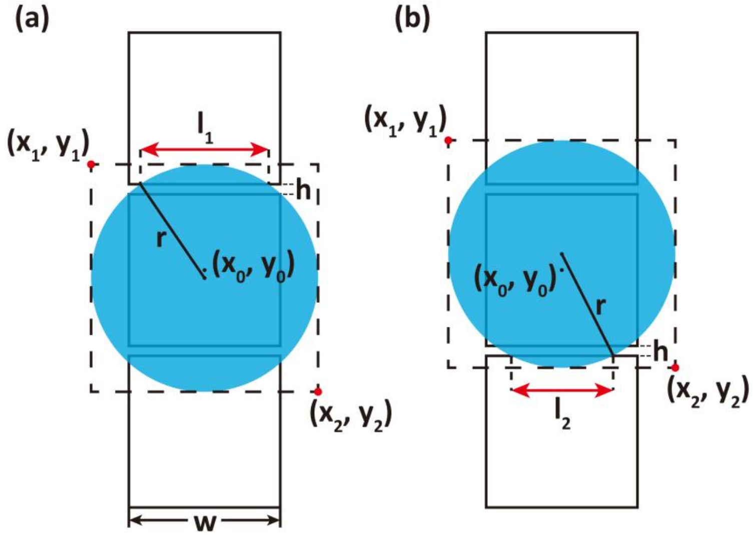

Fig. S5 Geometric relationship between contact line lengths and pixel coordinates. (a) The droplet is at a lower position. (b) The droplet is at a higher position.

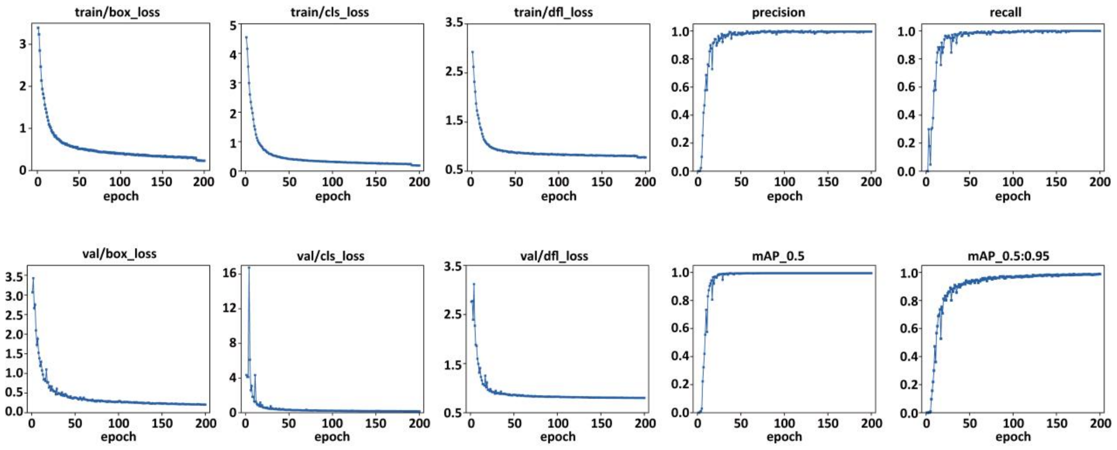

Fig. S6 Droplet detection performances on the training and validation sets. Train/box_loss is the bounding box regression loss during training. Train/cls_loss is the classification loss during training. Train/dfl_loss is the distribution focal loss during training. Precision is the proportion of predicted positive detections that are correct. Recall is the proportion of ground-truth objects that are correctly detected. Val/box_loss is the bounding box regression loss on the validation set. Val/cls_loss is the classification loss on the validation set. Val/dfl_loss is the distribution focal loss on the validation set. mAP_0.5 is the mean average precision at an IoU threshold of 0.5. mAP_0.5:0.95 is the mean average precision averaged over IoU thresholds from 0.5 to 0.95. After 150 epochs, all parameters converged to stable values. To avoid randomness, we calculated the average of each parameter over the final 50 epochs. On the training set, the bounding box regression loss is 0.345, the classification loss is 0.228, and the distribution focal loss is 0.818. On the validation set, the bounding box regression loss is 0.277, the classification loss is 0.184, and the distribution focal loss is 0.801. Furthermore, the mAP_0.5 is 0.995, the mAP_0.5:0.95 is 0.966, the precision is 0.995, the recall is 0.998, and the F1 score (equals to $2 * (precision * recall)/(precision + recall)$) is 0.996.

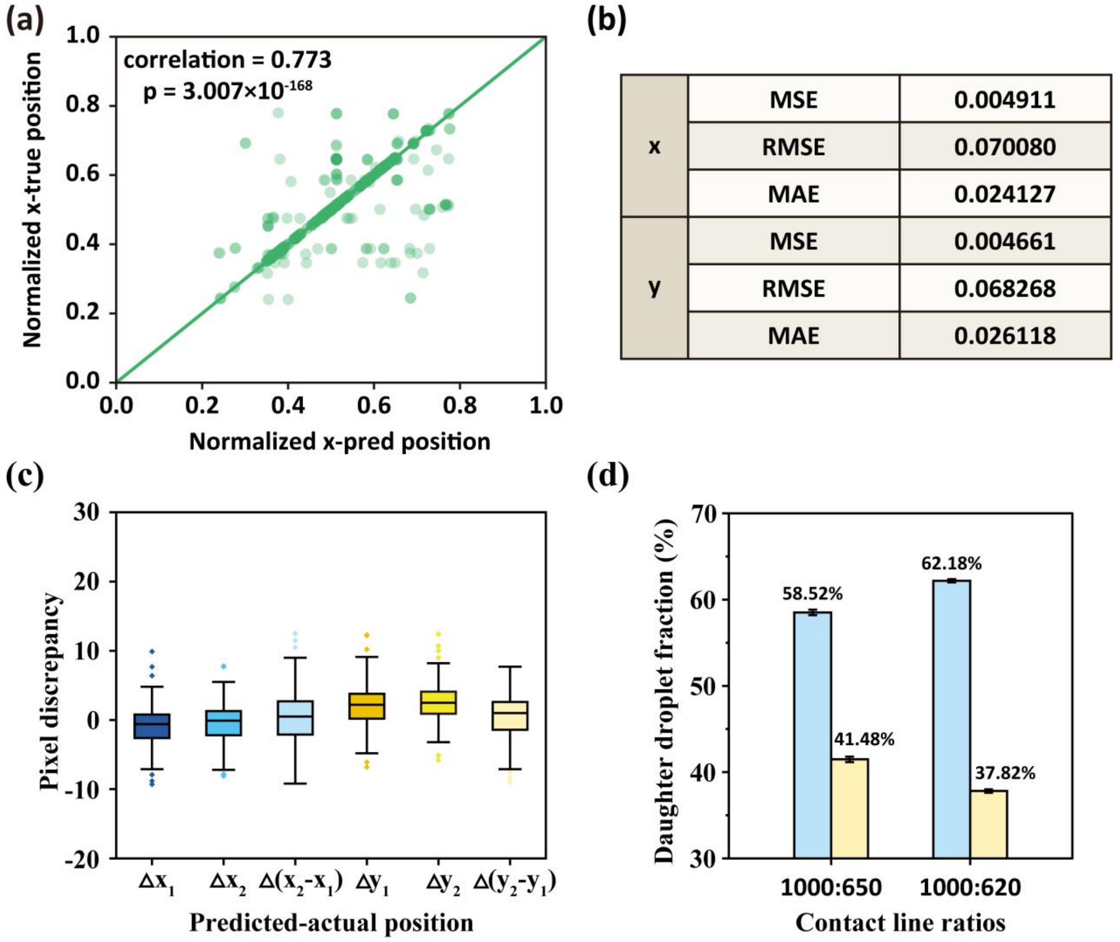

x	MSE	0.004911
	RMSE	0.070080
	MAE	0.024127
y	MSE	0.004661
	RMSE	0.068268
	MAE	0.026118

Fig. S7 (a) Scatter plot of the true and predicted droplet x-positions, with a total of 843 droplets detected. (b) Model prediction performance evaluation metrics. MSE is mean squared error. RMSE is root mean squared error. MAE is mean absolute error. (c) Box plot showing the accuracy of droplet position identification. The horizontal line inside the box represents the median; the box itself spans the interquartile range (IQR); and the horizontal lines extending from the top and bottom of the box indicate the maximum and minimum values of the data after excluding outliers. Where Δ donates the discrepancy between the pixel coordinates of the detection bounding boxes and the actual droplet positions. x_1 and x_2 represent the leftmost and rightmost x-coordinates of the droplets, respectively. y_1 and y_2 represent the upmost and downmost y-coordinates of the droplets, respectively. (d) Splitting results showing the volume fractions of the two daughter droplets at the contact line ratios of 1000:650 and 1000:620.

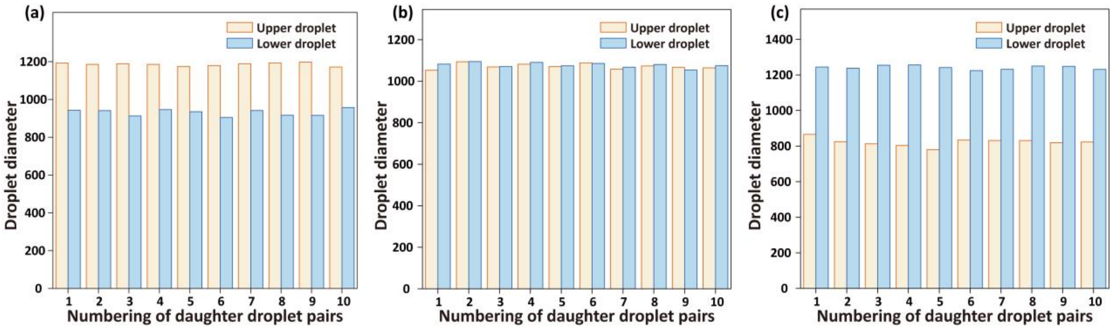

Fig. S8 Uniformity of droplets generated with automated splitting strategy. For contact line length ratios of (a) 1000:650, (b) 1000:750, and (c) 800:1000, the corresponding splitting ratios are 60:40, 50:50, 30:70, respectively.

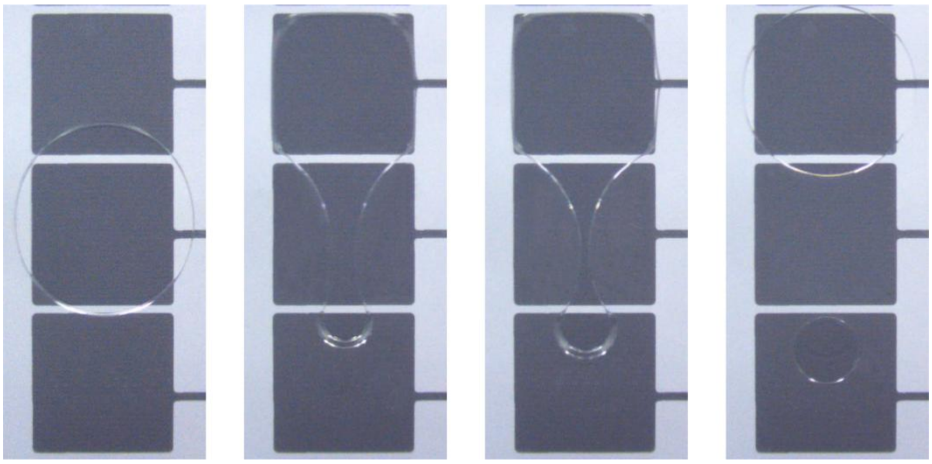

Fig. S9 The maximum sub-droplet ratio for gravity-assisted droplet splitting. In this work, the maximum splitting ratio reached up to 12:88 at the contact line ratio of 1000:280, the parent droplet diameter of 1300 µm, and the applied voltage of 170 Vpp.

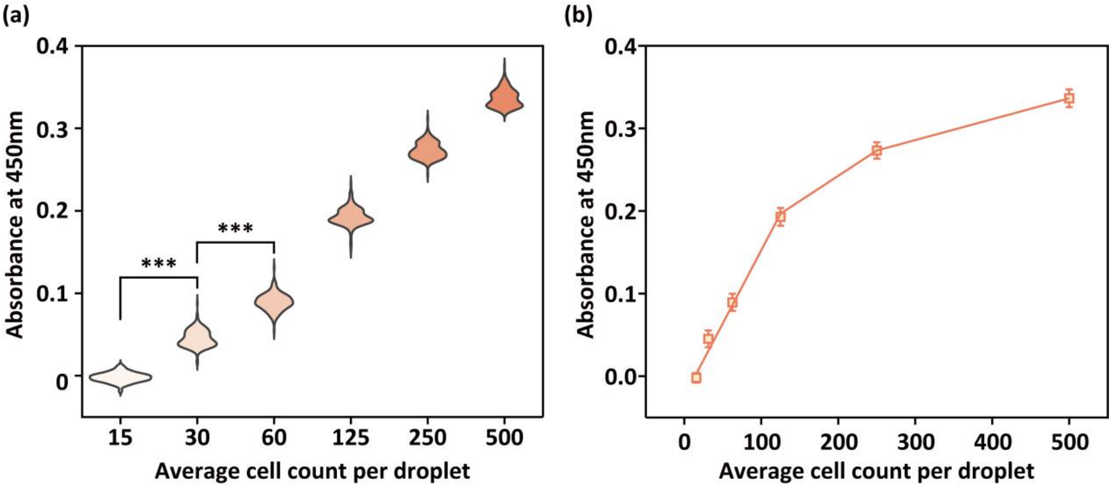

Fig. S10 On-chip cell quantification results. (a) Plot of absorbance versus the number of cells per droplet, showing that as few as 30 cells/droplet are detectable. Significant differences between groups were assessed using the Kruskal-Wallis H test (overall $p < 0.0001$) with Dunn's post hoc test (Bonferroni correction). * indicates $p < 0.001$. All pairwise comparisons between groups were highly significant (*p* < 0.001). (b) The line chart of droplet absorbance. When the number of cells within a droplet exceeds 140, the absorbance shows a significant deviation.

References

1. J. Berthier , P. Dubois , P. Clementz , P. Claustre , C. Peponnet and Y. Fouillet , Sens. Actuators, A, 2007, 134 , 471-479.

2. N.Sagar, S. Bansal and P. Sen, Advanced Materials Interfaces, 2022, 9, 2200240.

3. E. Samiei and M. Hoorfar, J. Micromech. Microeng., 2015, 25055008.

4. H. Wang and L. Chen, Nanotechnology Reviews, 2021, 10, 857-869.

5. K. Jin, C. Hu, S. Hu, C. Hu, J. Li and H. Ma, Lab Chip, 202121, 2892-2900.

6. Y.-H. Cheng, T.-J. Yang and Y.-W. Lu, Sensors Actuators B Chem., 2023, 390, 133989.

7. I. A. Eydelnant, U. Uddayasankar, B. B. Li, M. W. Liao and A. R. Wheeler, Lab Chip, 2012, 12, 750-757.

8. C. Dong, Y. Jia, J. Gao, T. Chen, P.-. Mak, M.-I. Vai and R. P. Martins, Lab Chip, 2017, 17, 896-904.

9. H. Li, R. Shen, C. Dong, T. Chen, Y. Jia, P.-I. Mak and R.P. Martins, Lab Chip, 2020, 20, 3709-3719.